

# Influence of interface roughness scattering on output characteristics of GaAs/AlGaAs quantum cascade laser in a magnetic field

M Žeželj<sup>1</sup>, V Milanović<sup>2</sup>, J Radovanović<sup>2</sup> and I Stanković<sup>1</sup>

<sup>1</sup> Scientific Computing Laboratory, Institute of Physics Belgrade, University of Belgrade, Pregrevica 118, 11080 Belgrade, Serbia

<sup>2</sup> School of Electrical Engineering, University of Belgrade, Bulevar kralja Aleksandra 73, 11120 Belgrade, Serbia

E-mail: milan.zezelj@ipb.ac.rs

Received 10 April 2011, in final form 30 June 2011

Published 27 July 2011

Online at [stacks.iop.org/JPhysD/44/325105](http://stacks.iop.org/JPhysD/44/325105)

## Abstract

We present a detailed theoretical analysis of LO-phonon and interface roughness scattering influence on the operation of GaAs/AlGaAs quantum cascade laser in the presence of an intense external magnetic field. The lifetime of the upper state, population inversion and optical gain show strong oscillations as a function of the magnetic field. These oscillations and their magnitude are found to be a result of the combined action of the two studied mechanisms and strongly influenced by temperature. At elevated temperatures, electrons in the relevant laser states absorb/emit more LO-phonons which results in reduction in the optical gain. We show that the decrease in the optical gain is moderated by the occurrence of interface roughness scattering, which remains unchanged with increasing temperature. Incorporation of the interface roughness scattering mechanism into the model did not create new resonant peaks of the optical gain. However, it resulted in shifting the existing peaks positions and overall reduction in the optical gain.

(Some figures in this article are in colour only in the electronic version)

## 1. Introduction

In recent years the scientific community has witnessed rapid progress in the development of unipolar semiconductor quantum cascade lasers (QCLs) [1–6]. In the mid- and far-infrared spectral range, these powerful light sources are particularly appreciated for the wide scope of operating wavelengths which can be achieved using the same heterostructure material combination. The wavelength tunability is realized by altering the active region design, i.e. modifying the layers' widths and composition [3–5]. The QCL emission is based on intersubband transitions between specific subbands within a multiple quantum well (QW) heterostructure. The typical design of the QCL active region entails a three-level system. An intense magnetic field parallel to the growth direction of semiconductor layers breaks the two-dimensional (2D) in-plane continuous energy spectrum into discrete Landau levels. This results in an increase of otherwise

short carrier lifetime (of the order of 1 ps) in the excited state [4–7]. The desired emission wavelength defines the necessary separations between the active laser energy states, while the spacing between the lower laser level and the ground state is set by LO-phonon energy. The lifetime of electrons in the excited laser state is strongly influenced and modulated by the applied magnetic field which results in oscillations in the laser emission intensity. Leuliet *et al* [6], attributed this effect to two scattering mechanisms: (1) inelastic scattering by LO-phonons and (2) elastic scattering by interface roughness. Given that the scattering processes between the two states depend on their energy spacing, certain relaxation mechanisms can be enhanced or inhibited by varying the magnetic field strength, although they may be influenced by the operating temperature as well. Hence, detailed understanding of various scattering mechanisms, relevant for laser operation, may be an important factor in improving its features and represents a key issue in efficient design of QCLs. LO-phonon scattering is well

explained in previous theoretical and experimental work [4, 8]. Increasing magnetic field reduces the number of levels under consideration and changes the energy differences between individual levels, thus affecting the lifetime of carriers in higher states. On the other hand, the influence of interface roughness scattering remained less clear. The strength of the interface roughness scattering in a particular sample is determined by the actual morphology of the interfaces. The common description of the effects of interface roughness scattering assumes a Gaussian correlation of interface steps with an average step height and a correlation length [6, 9–12]. In contrast to LO-phonon, interface roughness scattering does not depend on temperature. As a result, efficiency of the interface roughness scattering mechanism is expected to remain constant with increasing temperature, while the efficiency of LO-phonon scattering is reduced due to their higher absorption [13].

In this paper we study the electron relaxation rates for the upper state of the laser transition, due to electron–LO-phonon interactions and interface roughness scattering, for a structure subjected to a magnetic field parallel to the confinement direction. The QCL under consideration comprises a triple quantum well (TQW) GaAs/Al<sub>0.33</sub>Ga<sub>0.67</sub> and is intended for operation at 11.4 μm. To understand the effects of interface roughness scattering and compare it with LO-phonon scattering, we have studied relaxation times and optical gain for different temperatures and magnetic fields. The electron distribution over the states of the system is found by solving the full set of rate equations which describe the transitions between levels, and subsequently used to determine the optical gain.

In section 2, we present a theoretical description of realistic QCL active region and introduce models for LO-phonon scattering and interface roughness scattering rate in the presence of an external magnetic field. The rate equations which describe population change in each Landau level are presented as well. The stationary solution of these equations allows for evaluating the degree of population inversion and resulting optical gain. Section 3 brings calculations of the scattering rates and the total relaxation rate from the upper laser state, for a wide range of magnetic fields (3–60 T) and two temperatures  $T = 77$  K and 300 K. Using the calculated scattering rates as input data, rate equations are solved and population inversion and the optical gain are obtained. For both the population inversion and the gain, interface roughness scattering is shown to have a significant influence in terms of reducing the predicted magnitude, especially at low temperatures. Finally, in section 4 we discuss possible perspectives and continuation of the presented work.

## 2. Theoretical considerations

The active region of the QCL structure under consideration comprises three coupled QWs biased by an external electric field  $\vec{E}$  as displayed in figure 1. In the absence of the magnetic field this system has three energy states, i.e. subbands ( $n = 1, 2, 3$ ), and the laser transition occurs between subbands  $n = 3$  and  $n = 2$ . This active region is surrounded by suitable emitter/collector regions in the form of superlattices, designed as Bragg reflectors, which inject electrons into state  $n = 3$

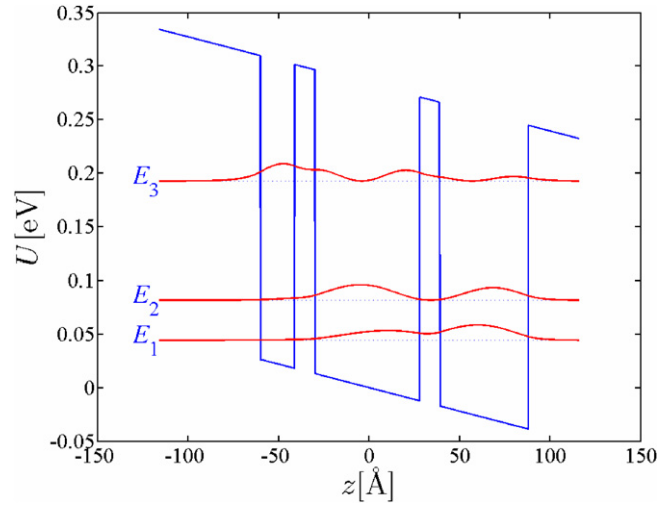


**Figure 1.** The conduction-band diagram of the active region of GaAs/Al<sub>0.33</sub>Ga<sub>0.67</sub>As QCL described in [4], in an electric field of 44 kV cm<sup>-1</sup>. The subband positions at zero magnetic fields, together with the corresponding wave functions squared, are also displayed.

on one side, and allow for rapid extraction of carriers from the lowest subband  $n = 1$ , on the other side. The energy difference between  $E_2$  and  $E_1$  should match the LO-phonon energy in order to ensure fast depopulation via LO-phonon scattering and maintain a short lifetime for the lower laser level. In addition, we introduce in our calculations the interface roughness scattering as additional nonradiative relaxation mechanism. The influences of these two mechanisms are compared in the following section.

The injection of carriers into the active region and extraction from the lower subband is achieved via resonant tunneling. In the absence of an external magnetic field, the electronic subbands from figure 1 have a free particle-like energy dispersion in the direction parallel to the QW planes  $E_n + \hbar^2 k_{\parallel}^2 / 2m_{\parallel n}(E_n)$ , where  $m_{\parallel n}(E_n)$  is the energy-dependent in-plane effective mass and  $k_{\parallel}$  is the in-plane wave vector. However, when this structure is subjected to a strong magnetic field  $B$  in the  $z$ -direction, continuous subbands transform into series of individual (strictly discrete) states, the total energies of which are [5]  $E_{n,l} \approx E_n + (l + 1/2)\hbar\omega_{c_n}$  where  $l = 0, 1, 2, \dots$  is the Landau index,  $E_n \equiv E_n(k_{\parallel} = 0)$ , the term  $(l + 1/2)\hbar\omega_{c_n}$  originates from the in-plane kinetic energy part of the subband, and  $\omega_{c_n} = eB/m_{\parallel n}$  is the corresponding cyclotron frequency. The values of  $B$  which give rise to resonant LO-phonon emission are found by solving the equation  $E_{3,0} - E_{n,l} = \hbar\omega_{LO}$  where  $n = 1, 2$ , while  $\hbar\omega_{LO}$  is the LO-phonon energy.

According to [6, 7], to account for the variations of the well widths, a Gaussian probability density is introduced:

$$\Pi(L_i) = \frac{1}{\sigma\sqrt{2\pi}} e^{-(L_i - L_{i0})^2 / 2\sigma^2}. \quad (1)$$

for the  $i$ th well width  $L_i$ ,  $i = 1, 2, 3$ . In order to keep the results as analytical as possible, we assume that around a mean value  $L_{i0}$  the energy difference varies linearly with  $L_i$ , i.e.

$$E_{n_i, l_i}(L_i) - E_{n_i, l_i}(L_{i0}) \approx E_{n_i, l_i}(L_{i0}) - E_{n_i, l_i}(L_{i0}) - \gamma(L_i - L_{i0}). \quad (2)$$

with the factor  $\gamma$  taken the same for all Landau levels, according to [6, 7].

By introducing equations (1) and (2) into the Fermi golden rule, we obtain the following function:

$$J^s = \int_{-\infty}^{\infty} \Pi(L_i) \delta[E_{n_i, l_i} - E_{n_f, l_f} - \Delta E_s] dL_i \\ = \frac{1}{\delta \sqrt{2\pi}} e^{-(E_{n_i, l_i} - E_{n_f, l_f} - \Delta E_s)^2 / 2\delta^2}, \quad (3)$$

where  $\delta = \sigma\gamma$  is the width of the Gaussian distribution of energy difference  $E_{n_i} - E_{n_f} + (l_i \omega_{c_{n_i}} - l_f \omega_{c_{n_f}}) \hbar + \hbar(\omega_{c_{n_i}} - \omega_{c_{n_f}})/2 - \Delta E_s$ , and  $s$  denotes the scattering mechanism (electron–LO-phonon scattering (LO) or interface roughness (IR) scattering). In our notation  $\Delta E_{LO} = \hbar\omega_{LO}$  and  $\Delta E_{IR} = 0$ . The terms  $E_{n, l}$  represent the total energies of Landau levels and a more detailed explanation of their calculation will be provided in the continuation of this section (equation (15)).

The electron–LO-phonon scattering rates for phonon emission between the initial state  $E_{n_i, l_i}$  and the final state  $E_{n_f, l_f}$  may be found from

$$\frac{1}{\tau_{(n_i, l_i) \rightarrow (n_f, l_f)}^{LO}} = \frac{2\pi}{\hbar} \sum_{\vec{q}} |\langle n_f, l_f, k_{x_f}, n_q + 1 | \hat{H}_{e-ph}(\vec{q}) | n_i, l_i, k_{x_i}, n_q \rangle|^2 J^{LO}. \quad (4)$$

In this expression, electron–LO-phonon Hamiltonian  $\hat{H}_{e-ph}(\vec{q})$  is the sum of the interaction Hamiltonian with each phonon mode defined by its 3D wave vector  $\vec{q}$ , see [7], and  $k_{x_i}$  and  $k_{x_f}$  are the initial and the final state wave vector components, respectively. From the previous equation one obtains the following analytical expression for scattering rate:

$$\frac{1}{\tau_{(n_i, l_i) \rightarrow (n_f, l_f)}^{LO, \{e\}}} = \frac{e^2 \omega_{LO}}{4\epsilon_0} \left( \frac{1}{\epsilon_\infty} - \frac{1}{\epsilon_s} \right) \\ \times \frac{1}{\delta \sqrt{2\pi}} e^{-(E_{n_i, l_i} - E_{n_f, l_f} - \hbar\omega_{LO})^2 / 2\delta^2} (n_q + 1) \\ \times \int_0^\infty |F(q_{\parallel})|^2 G(q_{\parallel}) dq_{\parallel}, \quad (5)$$

where  $\epsilon_\infty$  and  $\epsilon_s$  are the static and the high-frequency relative dielectric constant, respectively,  $\epsilon_0$  is the vacuum dielectric permittivity and  $n_q = [\exp(\hbar\omega_{LO}/k_B T) - 1]^{-1}$  is the mean number of LO-phonons.

Furthermore,  $q_{\parallel}$  is the in-plane component of the phonon wave vector  $\vec{q} = (q_z, q_{\parallel})$  and  $F(q_{\parallel})$  is the lateral overlap integral

$$|F(q_{\parallel}, l_i, l_f)|^2 = e^{-(q_{\parallel}^2 / 2\beta^2)} \frac{l_i!}{l_f!} \left( \frac{q_{\parallel}^2}{2\beta} \right)^{l_i - l_f} \left[ L_{l_i - l_f}^{l_i - l_f} \left( \frac{q_{\parallel}^2}{2\beta} \right) \right]^2, \quad (6)$$

where  $\beta = \sqrt{eB/\hbar}$  is the magnetic length and  $L_m^k(x)$  represents the associate Laguerre polynomial. Finally,  $G(q_{\parallel})$  stands for the form factor given by

$$G(q_{\parallel}) = \iint \eta_i^*(z) \eta_f(z) \eta_i(z') \eta_f^*(z') e^{-q_{\parallel}|z-z'|} dz dz', \quad (7)$$

where  $\eta_i$  and  $\eta_f$  denote the  $z$ -dependent parts of the electronic wave functions. The electron–LO-phonon scattering rate for phonon absorption [13] is

$$\frac{1}{\tau_{(n_f, l_f) \rightarrow (n_i, l_i)}^{LO, \{a\}}} = \frac{1}{\tau_{(n_i, l_i) \rightarrow (n_f, l_f)}^{LO, \{e\}}} \frac{1}{e^{\hbar\omega_{LO}/kT}}. \quad (8)$$

Phonon absorption is significant at room temperature ( $T = 300$  K) and it vanishes at low temperatures ( $T = 77$  K).

We use the model for interface roughness scattering proposed by Leuliet *et al*, cf [6]. This model assumes in-plane terrace-like surface defects, as explained in [14]. In order to evaluate the interface roughness scattering rate, we introduce spatial distribution of roughness which follows the Gaussian correlation function [6, 9–12]:

$$\langle \Delta(\vec{r}) \Delta(\vec{r}') \rangle = \Delta^2 e^{-|\vec{r} - \vec{r}'|^2 / \Lambda^2}, \quad (9)$$

with  $\Delta$  being the mean height of the roughness and  $\Lambda$  the correlation length. We also introduce the corresponding perturbation Hamiltonian [6],

$$\hat{H}_{IR} = U_0 \delta(z - z_i) \Delta(x, y), \quad (10)$$

where  $U_0$  is the barrier height at interface position  $z_i$ .

The electron-interface roughness scattering rate can be calculated from the following expression:

$$\left\langle \frac{1}{\tau_{(n_i, l_i) \rightarrow (n_f, l_f)}^{IR}}(z_i) \right\rangle \\ = \frac{2\pi}{\hbar} \left\langle \sum_{k_{x_i}, k_{x_f}} |\langle n_f, l_f, k_{x_f} | \hat{H}_{IR} | n_i, l_i, k_{x_i} \rangle|^2 \right\rangle J^{IR}. \quad (11)$$

In the above expression, the averaging is performed over space (as follows from equation (9)), and over the initial state wave vector component  $k_{x_i}$ . The interface roughness scattering takes place at all surfaces in the system, hence we can write the expression for the total scattering rate of the system from figure 1 as

$$\frac{1}{\tau_{(n_i, l_i) \rightarrow (n_f, l_f)}} = \frac{1}{\tau_{(n_i, l_i) \rightarrow (n_f, l_f)}^{LO}} + \sum_{z_i} \left\langle \frac{1}{\tau_{(n_i, l_i) \rightarrow (n_f, l_f)}^{IR}}(z_i) \right\rangle. \quad (12)$$

Finally, if one wants to compare the effects of electron–LO-phonon scattering and electron-interface roughness scattering, two things can be noted: (1) due to the nature of electron-interface roughness interactions, scattering rates for transition from lower to upper and from upper to lower energy level are equal. (2) the LO-phonon scattering has maximum influence when the energy difference between two states is close to phonon energy,  $\Delta E_{LO} = \hbar\omega_{LO}$ , on the other hand, the effects of interface roughness are maximal when the energy difference approaches zero. Therefore, the two mechanisms of scatterings are complementary.

The optical gain corresponds to transitions  $(3, l) \rightarrow (2, l)$  and is given by [8, 15]

$$g_{3 \rightarrow 2} = \frac{2e^2 \pi^2 d_{3 \rightarrow 2}^2}{\hbar \epsilon_0 \lambda} \sum_i \delta(E_{3, i} - E_{2, i} - \hbar\omega) (N_{3, i} - N_{2, i}), \quad (13)$$

where  $\bar{n}$  is the material refractive index,  $\lambda$  and  $\omega$  denote the wavelength and the frequency of the emitted light, respectively, while  $N_{3,i} - N_{2,i}$  represents the degree of population inversion. The transition matrix element is calculated as  $d_{3 \rightarrow 2} = \int \eta_3^*(z) z \eta_2(z) dz$ , where the wavefunctions  $\eta_n$  are found by solving the Schrödinger equation in the form [16]

$$\frac{d^2}{dz^2} \alpha_0 \frac{d^2 \eta_n}{dz^2} - \frac{\hbar^2}{2} \frac{d}{dz} \frac{1}{m} \frac{d \eta_n}{dz} + U(z) \eta_n = E_n \eta_n. \quad (14)$$

Here,  $m$  represents the effective mass at the conduction-band minimum. The energies  $E_{n,l}$  are given by Ekenberg as [16]

$$E_{n,l} = E_n + (l + 1/2) \frac{\hbar e B}{m_{\parallel n}} + [(8l^2 + 8l + 5) \langle \alpha_0 \rangle + (l^2 + l + 1) \langle \beta_0 \rangle] \frac{e^2 B^2}{2\hbar^2}. \quad (15)$$

In equation (15),  $m_{\parallel n}$  represents the parallel effective mass of the  $n$ th subband in the absence of the magnetic field [16]:

$$\frac{1}{m_{\parallel n}} = \int \eta_n^* \frac{1}{m} \eta_n dz - \frac{2}{\hbar^2} \int \eta_n^* \frac{d}{dz} (2\alpha_0 + \beta_0) \frac{d \eta_n}{dz} dz, \quad (16)$$

where  $\alpha_0$  and  $\beta_0$  are the nonparabolicity parameters.

To calculate the optical gain we need to find the inverse population which is the solution of a nonlinear system of rate equations:

$$N_i \sum_{j \neq i} \frac{\bar{f}_j}{\tau_{i \rightarrow j}} - \bar{f}_i \sum_{j \neq i} \frac{N_j}{\tau_{j \rightarrow i}} + \frac{J_i}{e} = 0, \quad (17)$$

where indices  $i, j = 1, 2, \dots$  denote the electronic states sorted by energy and

$$\bar{f}_i = 1 - \frac{\pi \hbar}{eB} N_i \quad (18)$$

is the probability that the state  $i$  is not occupied according to the Fermi–Dirac distribution. The electrons arrive in the active region from figure 1 by a constant current, and they are injected only into a limited number of Landau levels of the excited laser state, i.e. levels  $(3, 0), \dots, (3, l_{3,\max})$ . The injection current can be represented as a sum of all currents  $J_i$  which inject electrons into levels  $(3, l_3)$ , and in a similar manner, the extraction current can be expressed as a sum of all currents  $J_i$  which extract the electrons from levels  $(1, l_1)$ . The energy values of maximal Landau levels for each subband described by  $l_{1,\max}, l_{2,\max}$  and  $l_{3,\max}$ , are taken in this work to be roughly  $E_{3,0} + 5k_B T$  and it is reasonable to assume that these levels and the levels above are almost empty, cf [8].

### 3. Numerical results

The active region of a QCL based on GaAs/Al<sub>0.33</sub>Ga<sub>0.67</sub>As heterostructure, described in [4], designed to emit radiation at  $\sim 11.2 \mu\text{m}$ , is displayed in figure 1. The layer widths are 56, 19, 11, 58, 11, 49 and 28 Å, going from the emitter towards the collector barrier, and the electric field is 44 kV cm<sup>-1</sup>. The material parameters for GaAs used in the calculation are  $m = 0.067m_0$  and for Al<sub>0.33</sub>Ga<sub>0.67</sub>As  $m = 0.094m_0$  ( $m_0$  is the free electron mass),  $\bar{n} = 0.33$  and the conduction-band discontinuity between GaAs and

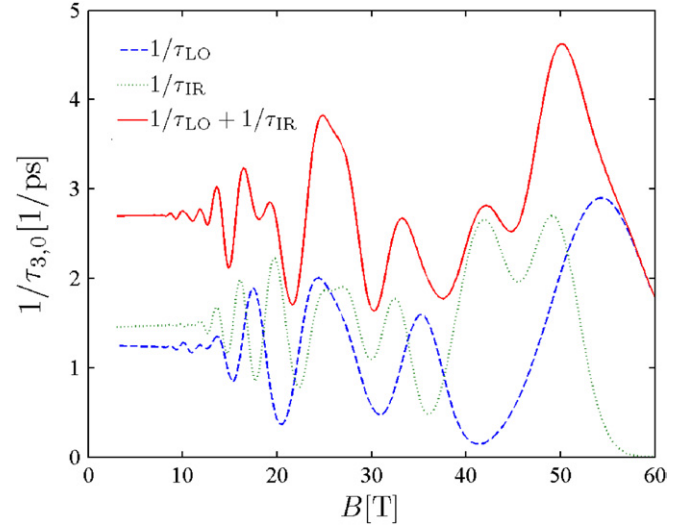


**Figure 2.** The total electron relaxation rate due to the electron LO-phonon scattering and interface roughness scattering for transitions from the ground laser level of the third subband into the two sets of Landau levels of the lower subbands, for magnetic fields in the range of  $B = 3\text{--}60$  T and at temperature  $T = 77$  K.

Al<sub>0.33</sub>Ga<sub>0.67</sub>As is  $\Delta E_c = 283.4$  meV. In the absence of magnetic field, the three subbands are at energies  $E_1 = 44.5$  meV,  $E_2 = 81.8$  meV and  $E_3 = 192.7$  meV, with the lasing transition energy of  $E_3 - E_2 = 110.9$  meV, in full agreement with experimental data [17]. Numerical parameters used in calculations are  $\varepsilon_\infty = 10.67$ ,  $\varepsilon_s = 12.51$ ,  $\hbar\omega_{\text{LO}} = 36.25$  meV,  $\delta = 6$  meV,  $\Delta = 1.5$  Å,  $\Lambda = 60$  Å and  $T = 77$  K and 300 K [6, 7]. The Dirac function in equation (13) is replaced by a Lorentzian with the linewidth parameter  $\Gamma = 4.25$  meV [18]. Nonparabolicity parameters  $\alpha_0$  and  $\beta_0$  are taken as  $-2107$  eV Å<sup>4</sup>, and  $-2288$  eV Å<sup>4</sup> for GaAs wells, and  $-1164$  eV Å<sup>4</sup>, and  $-1585$  eV Å<sup>4</sup> for Al<sub>0.33</sub>Ga<sub>0.67</sub>As barriers [16].

The scattering rate for the phonon absorption increases exponentially with temperature, cf equation (8). In the following text, we will therefore first present results for the low temperatures ( $T = 77$  K) when the phonon absorption is expected to be negligible and thereafter at room temperature ( $T = 300$  K) where it is significant.

The total relaxation rate for transitions from the ground Landau level of the third subband (into which the majority of carriers are injected) into the sets of Landau levels of the two other subbands is shown in figure 2, for the magnetic fields in the range of  $B = 3\text{--}60$  T and temperature  $T = 77$  K. Oscillations of the relaxation rate with  $B$  are very pronounced, and very prominent peaks are found at values of the magnetic field which satisfy the resonance conditions for LO-phonon emission. If the relaxation rates due to interface roughness and LO-phonon scattering are compared, one can see that the local relaxation rate maxima are of the same order of magnitude and not correlated with respect to the applied magnetic field. This is due to the fact that interface roughness scattering has the largest influence when the energy difference between states is diminishing. In contrast, for LO-phonon scattering, when the arrangement of laser levels is such that there is a level situated at  $\hbar\omega_{\text{LO}}$  below the state  $(3, 0)$ , this type of scattering

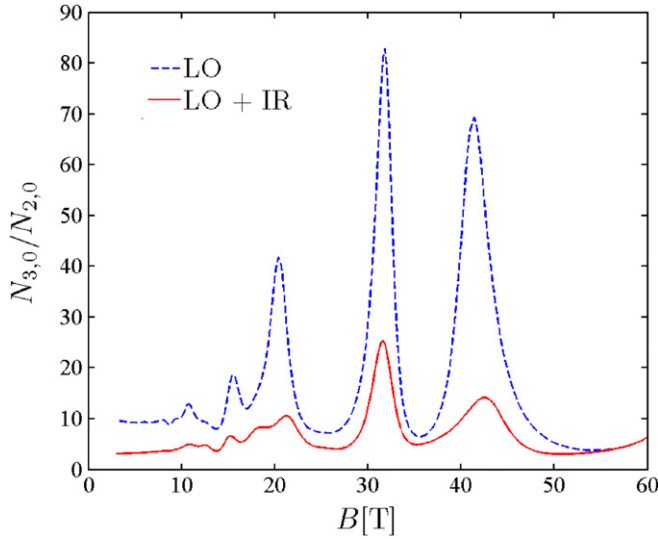


**Figure 3.** The ratio of the total electron areal densities due to the electron LO-phonon and interface roughness scattering, in the ground laser levels of the third and the second subband, as a function of the magnetic field and at temperature  $T = 77$  K.

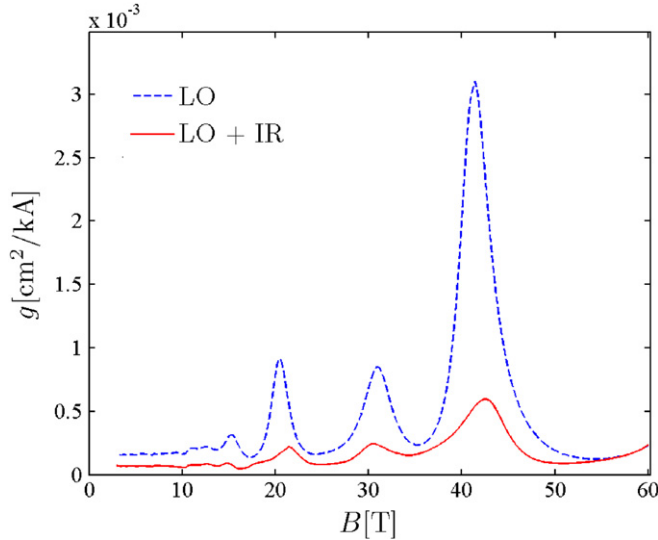


**Figure 4.** The optical gain (per unit injection current) as a function of the applied magnetic field in range  $B = 3\text{--}60$  T at temperature  $T = 77$  K.

is enhanced. One can also see that the peaks at magnetic fields  $B < 20$  T are a result of combined action of two scattering mechanisms. As already pointed out, the interface roughness scattering is enhanced when the energy spacing between levels is vanishingly small, while the LO-phonon scattering rates peak if this spacing is close to phonon energy. For that reason, at magnetic fields below 10 T, when the energy levels become dense, electron relaxation rates due to the interface roughness scattering exceed those of LO-phonon scattering.

Assuming a constant current injection, the modulation of lifetimes of all the states in the system results in either suppression or an enhancement of population inversion between states  $(3, 0)$  and  $(2, 0)$ , figure 3, and therefore in modulation of the optical gain per unit injection current  $g = g_{3,2}/J$  as well, figure 4. The first significant minimum

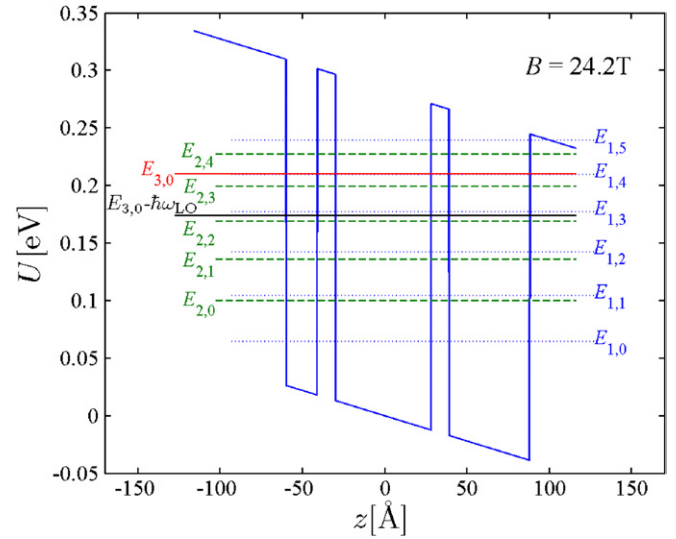


**Figure 5.** Positions of discrete states in the active region for the magnetic field of  $B = 24.2$  T, where the optical gain has a local minimum.

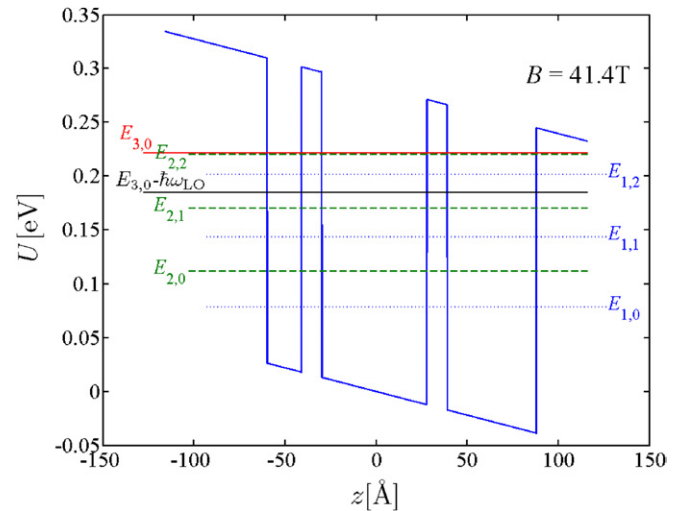


**Figure 6.** Positions of discrete states in the active region for the magnetic field of  $B = 41.4$  T, where optical gain has a maximum.

of the optical gain is at the magnetic field of  $B = 24.2$  T and the positions of relevant states in this case are displayed in figure 5. Electron relaxation from the state  $(3, 0)$  is maximized, see figure 2, because there are two states  $(2, 2)$  and  $(1, 3)$  with energies close to  $E_{3,0} - \hbar\omega_{LO}$ , together with the state  $(1, 4)$  very similar to  $(3, 0)$ , and the lifetime for the upper laser state is as low as  $\tau_{3,0} = 0.26$  ps. As a result of high relaxation rate, the inverse population is low, cf figure 3. Quite a different situation occurs at magnetic field around  $B = 41.4$  T. The configuration of relevant electronic states, shown in figure 6, leads to a maximally suppressed LO-phonon relaxation rate from  $(3, 0)$ , because there are no lower states with energy  $E_{3,0} - \hbar\omega_{LO}$  in the proximity, see figure 6. Still, since the scattering on interface roughness is also present, the maxima of inverse population and optical gain are shifted towards the higher values of the magnetic field ( $B = 42.5$  T). The calculated lifetime is  $\tau_{3,0} = 0.36$  ps. The most significant effect of the interface roughness scattering is the reduction in

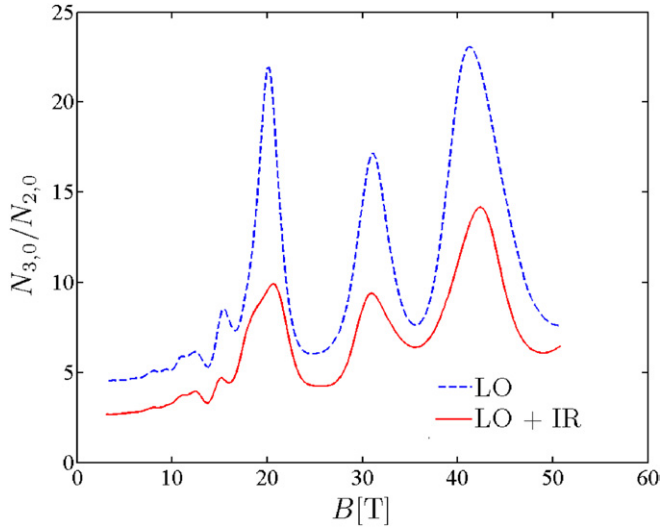


**Figure 7.** The ratio of the total electron areal densities due to the electron LO-phonon and interface roughness scattering, in the ground laser levels of the third and the second subband, as a function of the magnetic field and at temperature  $T = 300$  K.

the magnitude of inverse population, which results in reduced optical gain, cf, figures 3 and 4. Finally, we should note that introduction of interface roughness scattering did not create new resonant peaks. It only resulted in relatively small shift ( $\sim 1$  T) of the existing peaks.

At room temperature  $T = 300$  K, the total electron relaxation rate due to the electron LO-phonon scattering is higher ( $\sim 1.6$  times) than at temperature  $T = 77$  K. This increase in relaxation rate is caused by the temperature dependence of the distribution of phonon energies which enters equation (5). The increase in temperature has a significant effect on the reduction in inversion population due to intensified absorption of LO-phonons, as well as emission, which is evident from figure 7. At the same time, the scattering on interface roughness is independent of temperature. Consequently, the influence of interface roughness scattering on inversion population is less pronounced at higher temperatures, which can be verified by comparing the results obtained for the optical gain at 300 K, cf figure 8, with the results from figure 4.

Finally, we should note the QCL operating in the mid-IR spectral range was chosen to validate our model since experimental data were readily available [4]; however, the calculations could straightforwardly be modified for the THz spectral range, which we intend to focus on in our future work.

#### 4. Conclusion

We have set up a rate equation-based model and analysed the optical gain in the active region of a quantum cascade laser in a magnetic field perpendicular to the structure layers. The magnetic field alters the number of relevant in-plane electronic levels and the corresponding relaxation rates between them, by positioning some states on or off resonance with the upper laser level. In this work, LO-phonon and interface roughness scattering are compared. By examining the model itself, one

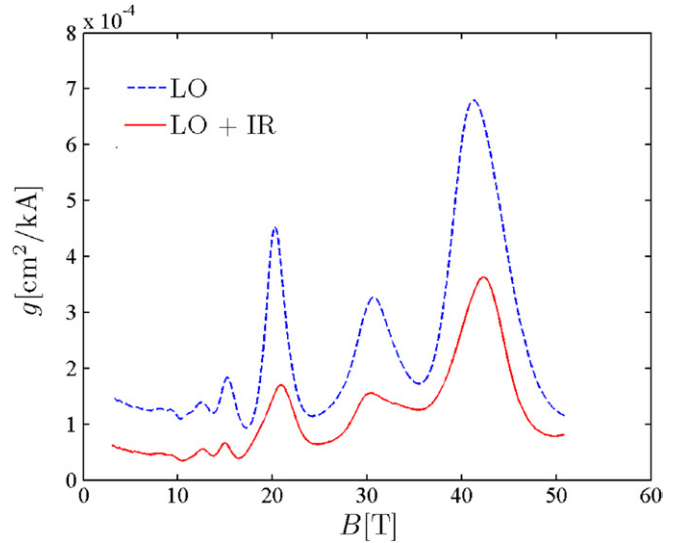


**Figure 8.** The optical gain (per unit injection current) as a function of the applied magnetic field in the range  $B = 3$ –60 T at temperature  $T = 300$  K.

could note that the interface roughness relaxation has maximal effects when the energy difference between levels is negligible. At the same time, the LO-phonon scattering is enhanced if energy difference is close to resonant phonon energy. From the numerical result it is evident that the inclusion of interface roughness scattering does not introduce additional peaks of inverse population and optical gain with varying magnetic field. However, for magnetic fields smaller than 10 T, when the energy levels become more closely spaced, the electron relaxation rates due to the interface roughness scattering become higher in comparison with LO-phonon relaxation rates. The most prominent effect of the interface roughness scattering is the overall reduction in the inverse population and the optical gain. Obviously, the operating temperature has an additional influence on the balance of the two scattering mechanisms. While the surface roughness scattering does not depend on the temperature, absorption/emission of LO-phonons increases exponentially with temperature. As a consequence, the optical gain resulting from the combined action of these scattering mechanisms is significantly reduced at higher temperatures.

#### Acknowledgments

MŽ and IS acknowledge support by the Ministry of Education and Science of the Republic of Serbia, under Project Nos III45018 and ON171017. Numerical simulations were run on the AEGIS e-Infrastructure, supported in part by FP7 projects EGI-InSPIRE, PRACE-IIP and HP-SEE. VM and JR acknowledge the support provided by the Ministry of Education and Science of the Republic of Serbia, Project No III 45010.

#### References

- [1] Faist J, Capasso F, Sivco D L, Sitori C, Hutchinson A L and Cho A Y 1994 *Science* **264** 553–6

- [2] Gmachl C, Capasso F, Sivco D L and Cho A Y 2001 *Rep. Prog. Phys.* **64** 1533–601
- [3] Becker C, Sirtori C, Drachenko O, Rylkov V, Smirnov D and Leotin J 2002 *Appl. Phys. Lett.* **81** 2941–3
- [4] Smirnov D, Drachenko O, Leotin J, Page H, Becker C, Sirtori C, Apalkov V and Chakraborty T 2002 *Phys. Rev. B* **66** 125317
- [5] Smirnov D, Becker C, Drachenko O, Rylkov V V, Page H, Leotin J and Sirtori C 2002 *Phys. Rev. B* **66** 121305
- [6] Leuliet A, Vasanelli A, Wade A, Fedorov G, Smirnov D, Bastard G and Sirtori C 2006 *Phys. Rev. B* **73** 085311
- [7] Becker C, Vasanelli A, Sirtori C and Bastard G 2004 *Phys. Rev. B* **69** 115328
- [8] Radovanović J, Milanović V, Ikončić Z, Indjin D and Harrison P 2005 *J. Appl. Phys.* **97** 103109
- [9] Ando T, Fowler a B and Stern F 1982 *Rev. Mod. Phys.* **54** 437–672
- [10] Unuma T, Yoshita M, Noda T, Sakaki H and Akiyama H 2003 *J. Appl. Phys.* **93** 1586–96
- [11] Califano N *et al* 2007 *Phys. Rev. B* **75** 045338
- [12] Valavanis A, Ikončić Z and Kelsall R W 2008 *Phys. Rev. B* **77** 075312
- [13] Teng H B, Sun J P, Haddad G I, Stroschio M A, Yu S and Kima K W 1998 *J. Appl. Phys.* **84** 2155–64
- [14] Weisbuch C, Dingle R, Gossard A C and Wiegmann W 1981 *Solid State Commun.* **38** 709–12
- [15] Živanović S, Milanović V and Ikončić Z 1995 *Phys. Rev. B* **52** 8305–11
- [16] Ekenberg U 1989 *Phys. Rev. B* **40** 7714–26
- [17] Kruck P, Page H, Sirtori C, Barbieri S, Stellmacher M and Nagle J 2000 *Appl. Phys. Lett.* **76** 3340–2
- [18] Wang J, Leburton J-P, Moussa Z, Julien F H and Sa'ar A 1996 *J. Appl. Phys.* **80** 1970–8